entropy

MDPI

Article

Sampling Quantum States with Inequality Constraints

Weijun Li [1,*], Rui Han [2], Jiangwei Shang [3], Hui Khoon Ng [4,5] and Berthold-Georg Englert [3,2,4]

[1] Department of Physics, University of Oxford, Oxford OX1 3RH, UK
[2] BiQut, Singapore 288564, Singapore; han.rui@quantumlah.org (R.H.)
[3] School of Physics, Beijing Institute of Technology, Beijing 100081, China; jiangwei.shang@bit.edu.cn (J.S.); berge@bit.edu.cn (B.-G.E.)
[4] Department of Physics, National University of Singapore, Singapore 117542, Singapore
[5] Centre for Quantum Technologies, Singapore 117543, Singapore; cqtnhk@nus.edu.sg (H.K.N.)
* Correspondence: liweijun2718@outlook.com

Abstract

Random samples of quantum states with specific properties are useful for various applications, such as Monte Carlo integration over the state space. In the high-dimensional situations that one already encounters when working with a few qubits, the quantum state space has a very complicated boundary, and it is challenging to incorporate the specific properties into the sampling algorithm. In this paper, we present the Sequentially Constrained Monte Carlo (SCMC) algorithm as a practical and versatile method for sampling quantum states in accordance with properties that can be stated as inequalities. We apply the SCMC algorithm to the generation of samples of bound entangled states; for example, we obtain nearly ten thousand bound, entangled, two-qutrit states in a few minutes, compared with less than ten such states per day from independence sampling in our implementation. In the second application, we draw samples of high-dimensional quantum states from a narrowly peaked target distribution and observe, for the system sizes investigated, that SCMC sampling remains computationally manageable as the dimensions grow. In yet another application, the SCMC algorithm produces uniformly distributed quantum states in regions bounded by values of the problem-specific target distribution; such samples are needed when estimating parameters from the probabilistic data acquired in quantum experiments.

Keywords: quantum state sampling; sequential Monte Carlo; sequentially constrained Monte Carlo; Markov chain; bound entanglement; positive partial transpose; computational cross norm; realignment; curse of dimensionality; target distribution; Wishart distribution

PACS: 02.50.Ng; 03.65.Aa; 03.65.Ud; 03.65.Wj

Academic Editor: Rosario Lo Franco

Received: 28 January 2026
Revised: 22 May 2026
Accepted: 26 May 2026
Published: 29 May 2026

1. Introduction

Random samples of quantum states with specific probability distributions and/or governed by specific physical properties are very useful for many applications in quantum information science and other research areas. For instance, they play an important role in quantum state and parameter estimation [1–3], allowing one to test and verify properties for certain classes of quantum states [4–6] as well as to test quantum channels and processes, such as the random quantum circuits leading to Quantum Supremacy [7–9]. Similar to sampling classical systems, independent rejection sampling methods are often inapplicable to high-dimensional quantum systems as they suffer severely from the exponential growth

of resource requirements, known as the "curse of dimensionality" [10]. The positivity boundaries of the quantum state spaces, moreover, are typically extremely complex to characterize for otherwise convenient parameterizations, causing quantum states to be more challenging to sample.

Most existing methods for the direct sampling of the random density matrices, which represent the quantum states numerically, rely on either clever parameterization of the state space or various kinds of induced measures [11–15]. The major drawback is that the exact probability distributions for random states constructed this way are usually not known; one has to estimate approximate distributions, and achieving this reliably is a numerical challenge in itself. Thus, rejection sampling methods that proceed from known proposal distributions are often still favored for sampling from a desired target distribution. However, even if one can directly draw from a reliable reference distribution that mimics the target distribution well—for example, using a version of the complex Wishart distribution [16–18]—the exponential reduction of the acceptance rate as the dimensions increase makes it rather impractical to go beyond sampling small quantum systems (see, for example, Reference [19]); other rejection sampling-based methods, such as adaptive rejection sampling, suffer from this problem, too.

Monte Carlo-based algorithms [20] can be much more resilient to this curse of dimensionality. The major difficulty encountered in using Monte Carlo (MC) methods comes from the incorporation of constraints into the parameter space. For instance, enforcing the positivity constraint needed for a physical state, which is intrinsic to quantum systems, can be extremely challenging. Algorithms that rely on clever random walks in the probability simplex, such as the Markov Chain Monte Carlo (MCMC), suffer from low acceptance rates because of this positivity constraint, and the Hamiltonian Monte Carlo (HMC) algorithm [21], whose random walk stays in the state space, depends on the evaluation of a Jacobian determinant and its derivatives, found to be numerically unreliable in high-dimensional quantum state spaces [22,23].

In this work, we investigate the use of Sequentially Constrained Monte Carlo (SCMC) samplers as a practical tool for sampling quantum states in accordance with a given distribution and/or certain physical properties, with particular emphasis on efficiently enforcing quantum constraints. SCMC samplers were first proposed by Golchi and Campbell in 2016 [24] to effectively impose constraints when sampling classical systems as an extension to the Sequential Monte Carlo (SMC) samplers proposed by Del Moral et al. a decade earlier [25]. SMC methods [26,27], which have been used extensively in the context of sequential Bayesian inference, are not new to the field of quantum information. For example, they have been well used in adaptive/online Bayesian Hamiltonian estimation [3,28,29]. In the context of sequential Bayesian inference, the sequence of distributions is constructed as more and more measurement data are taken into consideration. Unlike SMC methods in Bayesian inference, SMC samplers enable efficient sampling using MCMC algorithms through the introduction of a sequence of artificial intermediate distributions that bridge between an easy-to-sample initial distribution and the difficult-to-sample target distribution. One application of SMC samplers in quantum information science was recently presented in [30]. Here, we employ SMC samplers to sample quantum states, making use of SCMC samplers to better incorporate the constraints that naturally arise in quantum problems.

We study the performance of SCMC samplers for sampling quantum states through three concrete examples, which are otherwise difficult, or even impractical, to achieve using the standard existing methods mentioned above. In the first example, we show how SCMC samplers can be applied to sample quantum states with bound entanglement through the imposition of soft constraints. Large samples of uncorrelated bound entangled bipartite systems with dimensions 3×3, 3×4, 4×4, and 3×5 are reported, and a curious property

of the 2×4 system is observed. In this context, we note that the SCMC algorithm does not rely on a particular parameterization of the bound entangled state; see Section 3.1.

The second example presents a generic approach to sampling quantum states from desired target distributions. The efficiency and reliability of our algorithm is demonstrated via sampling three-qubit and four-qubit states. Moreover, within the range of system sizes considered, the results are consistent with a computational cost that grows much more mildly than what is typically encountered in direct rejection sampling.

In the last example, we sample uniformly distributed quantum states in regions bounded by the contours of the target distribution—uniform with respect to the volume elements induced by the Hilbert–Schmidt distance, that is. We improve on the implementation of the method recently introduced by Oh, Teo, and Jeong (OTJ) [31,32] and so confirm that the direct SCMC sampling from the target distribution is reliable. In addition, we observe that direct SCMC sampling is more efficient than the indirect OTJ method. Depending on one's point of view, the last example can be regarded as benchmarking SCMC against OTJ or OTJ against SCMC.

Some technical details are reported in the Appendix. Selected samples and codes can be fetched from a dedicated repository [33].

2. SCMC Sampling

The SMC samplers presented in Reference [25] enable one to sample $\mathbf{x}$ efficiently from its difficult-to-sample target distribution $f(\mathbf{x})$ through a sequence of intermediate distributions. We choose an initial distribution $g(\mathbf{x})$, which can be the prior or any appropriate reference distribution that is easy to sample from directly, and find a discrete sequence of N_τ density distributions $\big(h_i(\mathbf{x})\big)_{i=0}^{N_\tau}$ that smoothly bridges between $g(\mathbf{x})$ and $f(\mathbf{x})$. One particular choice of $h_i(\mathbf{x})$ is to follow the geometric path [34,35],

$$h_i(\mathbf{x}) = f(\mathbf{x})^{\tau_i} g(\mathbf{x})^{(1-\tau_i)}\,, \tag{1}$$

where τ_i runs from 0 to 1 in arithmetic progression, i.e., $\tau_i = i/N_\tau$ as i goes from 0 to N_τ. Thus, $h_0(\mathbf{x}) = g(\mathbf{x})$ and $h_{N_\tau}(\mathbf{x}) = f(\mathbf{x})$.

The utility of SMC samplers was extended by Golchi and Campbell [24] to SCMC samplers; in their approach the hard constraints on the parameter space are gradually incorporated into the intermediate distributions as soft probabilistic constraints. Here, soft constraints refer to relaxations that approach the hard constraint in the limit. For instance, when the desired hard constraint is $\kappa(\mathbf{x}) > 0$, with its indicator function being the step function $I_\kappa(\mathbf{x}) = \eta\big(\kappa(\mathbf{x})\big)$, the intermediate indicator functions for the soft constraints can be smooth approximations of the Heaviside step function, such as

$$I_{\kappa,i}(\mathbf{x}) = \frac{1 + \tanh\big(a\tau_i \kappa(\mathbf{x})\big)}{2}\,, \tag{2}$$

where the *tolerance* a is an adjustable scale controlling the *hardness* $a\tau_i$ of the constraint. In this case, the indicator function $I_{\kappa,i}(\mathbf{x})$ is incorporated into the SCMC sampler by taking

$$h_i(\mathbf{x}) \to h_i(\mathbf{x}) I_{\kappa,i}(\mathbf{x})\,, \tag{3}$$

and, within the limit of $a\tau_i \to \infty$, it converges to the hard constraint, i.e.,

$$I_{\kappa,N_\tau}(\mathbf{x}) \to \begin{cases} 1 \;\text{ for }\; \kappa(\mathbf{x}) > 0\,, \\ 0 \;\text{ for }\; \kappa(\mathbf{x}) < 0\,. \end{cases} \tag{4}$$

In practice, for a large but yet finite value of a, points with $\kappa(\mathbf{x}) \leq 0$ ($\kappa(\mathbf{x}) > 0$) are rejected (accepted) with a higher and higher probability as $\tau_i \to 1$; thus, sample points gradually move towards the region satisfying the constraint. At the final step of the SCMC algorithm, we impose the hard constraint instead of the probabilistic constraint and reject the sample points that violate the constraint. Between consecutive distribution steps, the sample is propagated by N_{MC} MCMC iterations, while the effective sample size is monitored to determine whether resampling is needed. We set N_{MC} sufficiently large, relative to the observed MCMC acceptance rate, so that each sample point is likely to move at least once between resampling events; once this condition is met, further increasing N_{MC} mainly increases CPU time and reduces residual correlations without noticeably changing the final sample in our examples. Consult the Appendix for implementation details.

The ability to enforce constraints via SCMC is very useful for sampling quantum states because the quantum Hilbert space intrinsically requires the physicality constraint, which usually means complicated constraints on the parameters (positivity of a large matrix) that are CPU expensive to check. Apart from the physicality constraint, many other interesting quantum constraints can also be extremely difficult to enforce as suitable parameterizations of the states are unavailable. For efficient sampling of quantum states, we need to identify the quantum constraints and find their corresponding indicator functions. Next, we show how well the SCMC sampler works for sampling quantum states in three distinct contexts.

3. Examples

3.1. Bound Entanglement

A bound entangled state is a state with non-distillable entanglement. It has drawn a lot of attention in the quantum information community since the prediction of its existence in 1998 [36]; see [37] for a recent review. Random samples of bound entangled states are useful not only for the field of quantum information but also for mathematical interests. On the one hand, states with bound entanglement provide a testbed for studying the relationship between entanglement, steering, and Bell-type nonlocality [38,39]; on the other hand, bound entangled states enable the study of positive maps from a different perspective [40]. Moreover, despite being highly mixed, such states are potentially useful for quantum cryptography and quantum metrology [41,42].

While it is currently unknown if all bound entangled states have a positive partial transpose (PPT), we do know that all entangled PPT states are bound entangled [36], and a PPT state is surely entangled if the computable cross norm or realignment (CCNR) criterion is met [43]. Taken together, then, the two conditions

$$\min\{\mu_{\mathrm{PT}}\} \geq 0 \quad \text{and} \quad \sum_j \sigma_j(\tilde{\rho}) \equiv R > 1 \tag{5}$$

are sufficient to ensure bound entanglement. Here, $\{\mu_{\mathrm{PT}}\}$ is the set of eigenvalues of the partial transpose of the density matrix ρ, and R is the sum of the singular values of the realigned matrix $\tilde{\rho}$; see Equation (5) in Reference [43]. Examples of bound entangled states are studied in the literature; see, for example, References [36,38,44–50]. They are often given as special constructions of states in some particular parameter families. A more general way of constructing bound entangled states which allows the generation of a random sample has also been presented in Reference [51], but it only works for bipartite systems with equal dimensions.

The SCMC samplers are well suited for generating random samples of PPT bound entangled states with no restrictions on the states' parameter family or on their dimensionality. They can be generated by imposing the two criteria in Equation (5) in the same way as one imposes the physicality constraint. The two indicator functions are in the form of

Equation (2) with $\kappa_1(\rho) = \min\{\mu_{\mathrm{PT}}\}$ and $\kappa_2(\rho) = R - 1$, respectively. The initial reference sample of dimension d can be drawn directly from a uniform distribution of physical states using the Wishart distribution $W_d^{(\mathrm{Q})}(d, \mathbf{1}_d)$, that is, they are generated from $d \times d$ normally distributed complex matrices with mean zero and covariance matrix $\mathbf{1}_d \otimes \mathbf{1}_d$ (see Reference [19] for more details). Since the reference samples are physical initially, and we do not want to have unphysical sample points as the samples are processed, we impose hard physicality constraints during the Markov chain steps to ensure that the random walks do not move a quantum state beyond the physical boundary. Examples illustrating the generation of random samples of bound entangled states are shown in Figure 1, where the states in the initial reference sample are represented by red crosses and the sample states after SCMC and before the final rejection sampling are represented by blue dots. As is clearly visible from the plots, our SCMC sampler successfully moved the states toward the region around $R = 1$ and $\min\{\mu_{\mathrm{PT}}\} = 0$ and produced bound entangled states. Table 1 lists the parameters used for the SCMC sampling together with the yield of bound entangled states and the CPU time consumed in each distribution step.

Table 1. Parameters used for the SCMC sampling ($\times \rightarrow \bullet$) reported in Figures 1 and 2: number N_τ of intermediate distributions, tolerance a_e for the entanglement constraint, tolerance a_p for the PPT constraint, yield of bound entangled states, and CPU time per distribution step.

System	N_τ	a_e	a_p	Yield	Time
3×3	20	1,000	10,000	85%	11 s
3×4	2,000	1,000	10,000	70%	14 s
3×5	2,000	3,000	20,000	22%	15 s
4×4	2,000	3,000	500,000	40%	22 s
2×4	20	200	300	0%	7 s

As discussed in the previous section, the efficiency of SCMC depends on a number of parameters, including the tolerance a_p for the PPT constraint, the tolerance a_e for the CCNR entanglement constraint, and the number N_τ of the distribution steps. These tuning parameters are strongly problem dependent; their useful ranges vary with the dimension, target distribution and the particular constraints, as is also reflected by the wide ranges for a_e and a_p in Table 1. In this feasibility study, we therefore select them empirically, using the final rejection yield and the computational time as practical diagnostics rather than attempting a universal optimization rule.

Rejection sampling is applied to impose the complete set of hard constraints at the end of the algorithm; thus, a good set of the parameters should result in a high yield of accepted sample points within reasonable CPU time. For the bipartite qutrit system of dimension $d = 3 \times 3$, a 99% yield of bound entangled states was obtained by setting $N_\tau = 300$ and $a_e = a_p = 5 \times 10^4$. On our standard desktop, it took a few minutes to find thousands of two-qutrit bound entangled states; CPU parallelization is possible and will speed up the computation. For comparison, we conducted independent sampling by drawing 10^{10} states from a uniform distribution of bipartite qutrit states. Only 24 out of the 10^{10} states obeyed the criteria of Equation (5), and this process took days even with CPU parallelization. Such a search for higher-dimensional systems (3×4, 3×5, or 4×4, say) is even more difficult. This illustrates a substantial practical improvement provided by the SCMC algorithm for this task.

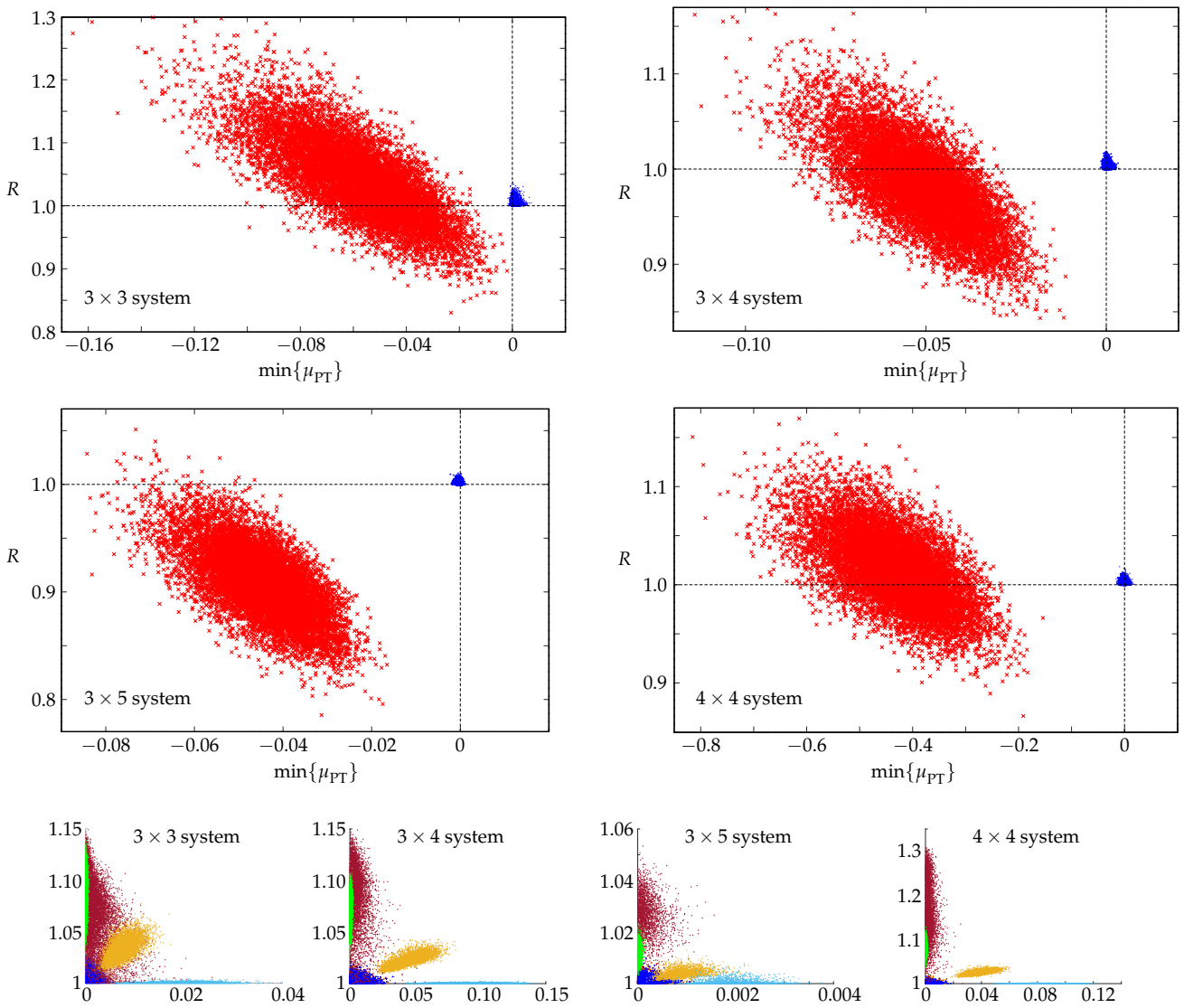

Figure 1. The generation of bound entangled states using SCMC. The initial reference sample has 10^4 states (red crosses) uniformly distributed with respect to the Hilbert–Schmidt distance shown here on an R vs. $\min\{\mu_{\mathrm{PT}}\}$ plot. The states after SCMC are indicated by the blue dots. Out of these 10,000 post-SCMC states, 8530, 7011, 2211, and 4013 states are bound entangled for the respective systems of dimensions 3×3, 3×4, 3×5, and 4×4. The plots in the bottom row show samples in the first quadrant, where the double criterion of Equation (5) is obeyed, filtered through further MCMC iterations, with different colors representing different propagation kernels (by choosing different directions of the random walks).

In Figures 1 and 2, we show scatter plots of the $\min\{\mu_{\mathrm{PT}}\}$ and R values of samples obtained by SCMC for five systems with Hilbert-space dimensions between eight and sixteen (state space dimensions between 63 and 255). No exhaustive trials were conducted, and the performance can certainly be improved upon, as we did not optimize the parameters. Since we are imposing the constraints through the two inequalities in Equation (5), the states produced were clustered in the small corner near $R = 1$ and $\min\{\mu_{\mathrm{PT}}\} = 0$ for the four systems in Figure 1, but not for the 2×4 system in Figure 2. For the cases of Figure 1, to explore other parts of the space for larger values of R and $\min\{\mu_{\mathrm{PT}}\}$, we filtered the sample further through MCMC iterations with different kernels and acceptance criteria, such as "accept only if R is increased;" the samples obtained are shown in the the bottom row of Figure 1. This way of producing random samples of bound entangled states, without re-

lying on special constructions of parameter families of states, will be very useful when studying general properties of bound entanglement; such investigations are, however, not the objective of this work.

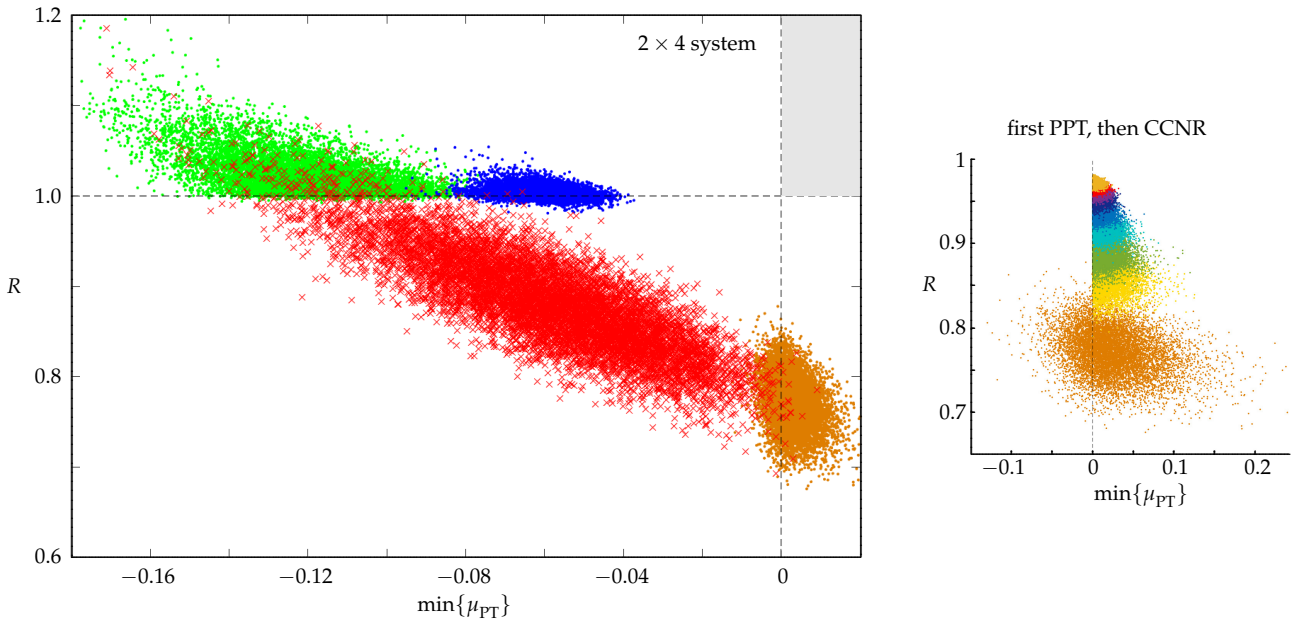

Figure 2. Search for bound entangled states with SCMC for the 2×4 system. **Left:** The initial reference sample has 10^4 states (red crosses) uniformly distributed with respect to the Hilbert–Schmidt distance shown here on an R vs. $\min\{\mu_{\mathrm{PT}}\}$ plot. The states after SCMC are indicated by the blue dots. There are no blue dots in the first quadrant (gray) where the criteria (5) are obeyed. Enforcing only the PPT criterion results in the orange sample; enforcing only the CCNR criterion results in the green sample. **Right:** The orange sample is shown together with, in different colors, further samples that are obtained by SCMC steps toward enforcing the CCNR criterion.

The 2×4 system of Figure 2 is particular—we could not find any states that satisfy both the PPT and the CCNR criterion in (5). When either one of the criteria is enforced, SCMC yields samples with $\min\{\mu_{\mathrm{PT}}\} \geq 0$ or $R > 1$, respectively. As the plot on the right in Figure 2 shows, first enforcing the PPT criterion, followed by SCMC steps toward enforcing the CCNR criterion, produces samples with R values that are sequentially closer to the $R = 1$ threshold without, however, crossing it. We conjecture that 2×4 systems do not have bound entangled states that obey the sufficient double criterion of (5). There are, of course, bound entangled states that do not obey these criteria. Indeed, the families of bound entangled 2×4 states constructed by the authors of [44,47,48] are PPT with $R \leq 1$; their values are on the straight lines with endpoints $(\min\{\mu_{\mathrm{PT}}\}, R) = (0, 1)$ and $(0, 0.7866)$, $(0, 0.8727)$ and $(0.0270, 0.7572)$, or $(0, 1)$ and $(0, 0.8536)$, respectively. In Figure 2, they are all on, or very close to, the dashed vertical line at $\min\{\mu_{\mathrm{PT}}\} = 0$.

These examples illustrate that the criteria (5) are not necessary—the pair is sufficient. It is possible, perhaps likely, that the final SCMC samples (blue dots in Figures 1 and 2) contain bound entangled states outside the first quadrant, but the yields reported in Table 1 refer solely to the states that meet the double criterion.

3.2. Desired Target Distribution

Random samples from a desired distribution are useful in various contexts in quantum information science such as studying properties of a quantum system, parameter optimization, or model testing. Owing to the notorious curse of dimensionality and/or quantum constraints, sampling methods that work well for low-dimensional systems fail

to work in practice as the dimensions increase. (The curse refers to the dimensionality of the parameter space, not of the Hilbert space.) For example, the generation of a target sample from a uniform reference distribution of states through rejection sampling fails to work for three-qubit systems, as the acceptance rate is extremely low; one can increase the acceptance rate by orders of magnitude by replacing the uniform reference sample with an appropriate Wishart distribution of states. Nevertheless, the efficiency still suffers from an exponential decay with respect to dimensionality [19]. On the other hand, Markov chain algorithms suffer from instability and their unavoidable sample correlation [22,23]. In this section, we demonstrate that SCMC can be used for generating samples of a desired target distribution at high dimensions, impractical otherwise, and, for the system sizes investigated, the computational cost does not show the severe exponential deterioration characteristic of direct rejection sampling.

To be specific, we consider the generic situation where the desired distribution is of the Dirichlet form

$$f(\rho) \propto \prod_k \mathrm{tr}\big(\Pi_k \rho\big)^{\alpha_k} = \prod_k p_k^{\alpha_k}, \quad \rho > 0\,, \tag{6}$$

which is central to quantum state estimation with a conjugate prior. The probability operators Π_k have the usual properties, namely $\Pi_k \geq 0$ and $\sum_k \Pi_k = \mathbf{1}$, and the set $\mathbf{\Pi} = \{\Pi_k\}$ is an informationally complete measurement so that there is a one-to-one correspondence between the state ρ and the probabilities $\mathbf{p} = \{p_k\} = \mathrm{tr}\big(\mathbf{\Pi}\rho\big)$. Note that a sample drawn from the Dirichlet distribution by one of the standard efficient algorithms, which draw from the probability simplex, has many unphysical entries ($p_k > 0$ while $\rho \ngeq 0$), and simply discarding them would results in a very poor yield. The SCMC procedure pushes most of the initially unphysical sample points into the physical state space. Similar remarks apply to samples drawn from a Dirichlet distribution centered at the state for which $f(\rho)$ is largest, which is often a rank-deficient state. Note also that the Dirichlet distribution has a single very narrow peak when $A = \sum_k \alpha_k$ is large, as is the typical situation in quantum state estimation scenarios.

To apply SCMC, we first need a set of initial sample points that can be easily generated. Conventional MC methods often use samples generated in the probability simplex, such as the Dirichlet distribution, that do not respect the positivity constraints, but the rate of physical samples decreases exponentially with respect to the dimensions of the parameter space, which makes it impractical for high-dimensional systems (for example, the physical rate is less than 10^{-10} for a three-qubit system [19]). Therefore, for efficient sampling, it is expedient to use an initial reference sample that is physical. We mainly explore two types of initial reference sample distributions: the uniform distribution with respect to the Hilbert–Schmidt distance and the peaked Wishart distribution. The former rarely resembles any feature of the target distribution, but the intermediate distributions $\{h_i(\rho)\}$ are straightforward to evaluate for each sample point in the algorithm. The Wishart distribution for quantum states $W_d^{(\mathrm{Q})}(n, \Sigma)$ offers more freedom by adjusting the covariance matrix Σ in shaping the reference distribution towards a target while conforming to the physicality constraint. Its probability density for a d-dimensional system is [19]

$$g(\rho) \propto \frac{\det(\rho)^{n-d}}{\mathrm{tr}\big(\Sigma^{-1}\rho\big)^{nd}}\,, \tag{7}$$

where $\rho = Z^\dagger Z / \mathrm{tr}\big(Z^\dagger Z\big)$ and the $d \times n$ random complex matrix Z, with $n \geq d$, is drawn from a Gaussian distribution with zero mean and covariance matrix $\mathbf{1}_n \otimes \Sigma$; we get the uniform distribution for $n = d$ and $\Sigma = \mathbf{1}_d$. We expect faster convergence using the Wishart distribution, as it is more similar to the target distribution. However, the apparent downside

is that the numerical evaluation of its initial and resulting intermediate distributions takes longer.

To test its performance, we run the SCMC algorithm for different numbers of intermediate distributions N_τ and different types of initial reference distributions. We assess the quality of the sample by a variant of the method described in Section 5 of Reference [19], for which we introduce the nested λ-regions with $f(\rho) \geq \lambda F$, where $F = \max_\rho\{f(\rho)\}$ is the peak value of $f(\rho)$, and $0 \leq \lambda \leq 1$. We have the full physical state space for $\lambda = 0$ and only the peak location for $\lambda = 1$. The fraction of the target distribution contained in a λ-region is its *content* c_λ:

$$c_\lambda = \int (\mathrm{d}\rho)\, f(\rho)\eta\big(f(\rho) - \lambda F\big)\,, \tag{8}$$

where $c_{\lambda=0} = 1$ reflects the normalization of $f(\rho)$ to unit integral. By counting how many sample points are inside a λ-region, we obtain an estimate for the respective c_λ value. Note that, in the context of Bayesian estimation, c_λ is the credibility of the region, if $f(\rho)$ is the posterior distribution.

We expect that this estimate is better (i) when more intermediate steps N_τ are used in the SCMC algorithm and (ii) when the sample size N_s is larger. Both expectations are confirmed by the data presented in Figure 3 for two examples, one for a three-qubit system and one for a four-qubit system. The two $f(\rho)$s are posterior distributions (for a uniform prior) for $A = 3000$ randomly generated measurement clicks of product tetrahedron measurements.

With this large A value, the distributions are squeezed into a tiny region in the immediate vicinity of the peak location of $f(\rho)$ at or near the boundary of the state space, which makes them impractical for sampling with conventional methods. In the SCMC algorithm, besides imposing the sequence of intermediate distributions to approach the desired one gradually from the reference distribution, the physicality constraints also have to be imposed either strictly or gradually. When the initial sample points are guaranteed to be physical, such as the ones uniformly drawn from the state space, the hard physicality constraint is directly imposed during the MCMC iterations. Otherwise, when a portion of the initial sample distribution is unphysical, as in the case of the linearly shifted Wishart distribution [19] or the Dirichlet distributions, we impose the soft physicality constraint gradually along with the distribution steps. Note that, when the constraint is strictly imposed throughout, one could make use of a Cholesky decomposition to check for a semi-positive-definite and hermitian matrix; then, the positivity of the smallest eigenvalue of the matrix corresponding to ρ is used to impose the soft constraint via the indicator function.

In the three-qubit example shown in Figure 3a, we find it sufficient to have $N_\tau = 300$ intermediate steps when the initial sample is drawn from an appropriate Wishart distribution, as the content barely changes by increasing N_τ further. When $N_\tau = 100$, the Dirichlet distribution centered at the peak of $f(\rho)$ performs the best, and the uniform distribution performs the poorest. Their difference becomes less and less noticeable with increasing number of distribution steps. For example, no significant difference is shown in their performance when $N_\tau = 150$. Thus, it is evident that the SCMC algorithm tolerates flexibility in the choice of the initial reference distribution, although a reference distribution that better resembles the target can offer faster convergence.

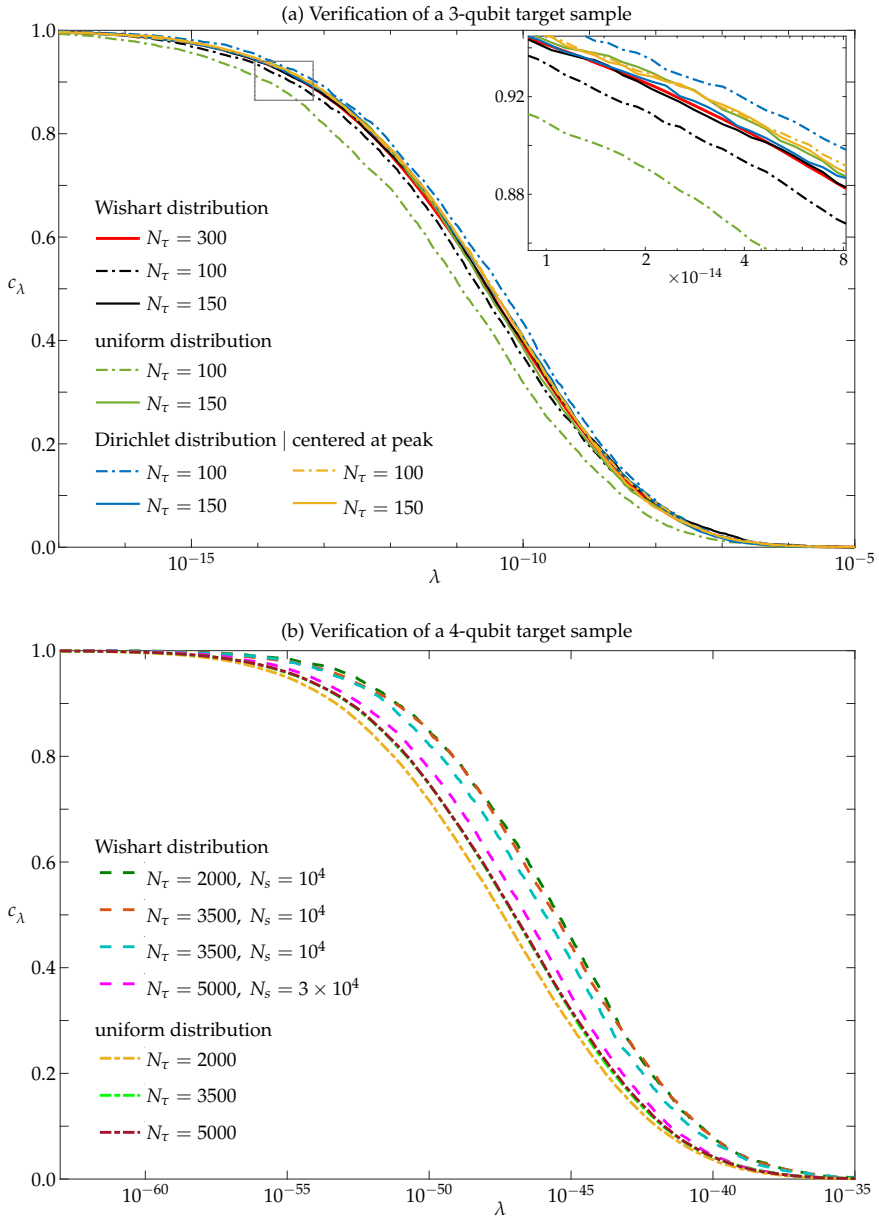

Figure 3. The content c_λ evaluated for samples generated for (**a**) a three-qubit target distribution and (**b**) a four-qubit target distribution. The target distributions are given by $A = 3000$ randomly generated detection events for product tetrahedron measurements. The samples are obtained using SCMC with N_s initial reference points drawn from the Wishart distribution, the uniform distribution, the Dirichlet distribution, or the Dirichlet distribution centered at the peak of $f(\rho)$. The SCMC algorithm is run for different numbers of intermediate distributions N_τ. The inset in (**a**) is a blow-up of the marked rectangular area. In lexicographic order, the counts of the simulated product tetrahedron measurements detection events that make up the data for the target distributions are as follows: for the three-qubit example, {36, 13, 64, 71, 14, 16, 7, 15, 60, 10, 84, 63, 64, 9, 55, 71, 8, 12, 10, 16, 16, 48, 67, 62, 9, 64, 75, 63, 10, 74, 60, 73, 65, 14, 62, 66, 9, 57, 76, 53, 82, 78, 128, 22, 61, 44, 25, 27, 56, 12, 52, 66, 14, 76, 56, 78, 45, 47, 22, 27, 66, 68, 25, 102}; and the four-qubit example, {5, 5, 11, 9, 5, 6, 3, 5, 11, 4, 18, 18, 11, 3, 10, 24, 5, 4, 2, 5, 1, 5, 1, 2, 2, 1, 3, 1, 5, 6, 3, 4, 16, 3, 24, 15, 3, 4, 4, 0, 16, 4, 27, 14, 13, 1, 17, 20, 9, 4, 16, 16, 4, 2, 2, 4, 21, 3, 27, 23, 19, 4, 18, 35, 2, 3, 1, 6, 4, 0, 4, 5, 4, 6, 7, 4, 3, 3, 1, 6, 0, 4, 4, 4, 0, 15, 14, 5, 2, 5, 19, 17, 3, 8, 14, 12, 2, 2, 2, 2, 2, 16, 13, 13, 3, 26, 26, 21, 7, 27, 13, 13, 2, 1, 2, 4, 2, 8, 17, 21, 2, 23, 21, 13, 4, 24, 21, 18, 7, 5, 17, 19, 4, 1, 9, 1, 10, 3, 25, 17, 19, 4, 15, 18, 1, 6, 1, 1, 3, 15, 15, 17, 3, 20, 26, 21, 1, 15, 21, 17, 14, 5, 41, 16, 10, 14, 40, 23, 35, 22, 71, 20, 14, 17, 22, 3, 13, 0, 16, 17, 1, 9, 12, 23, 16, 17, 20, 1, 14, 27, 2, 17, 12, 3, 17, 20, 4, 6, 4, 3, 17, 4, 19, 13, 17, 3, 14, 21, 5, 5, 4, 6, 3, 13, 11, 18, 1, 17, 20, 19, 2, 20, 19, 26, 21, 4, 20, 21, 3, 24, 22, 14, 18, 17, 22, 4, 15, 17, 6, 14, 18, 6, 11, 21, 4, 24, 18, 28, 18, 16, 0, 21, 30, 28, 11, 67}.

Figure 3b shows the content of the four-qubit samples generated starting from either a Wishart distribution or a uniform distribution. The Dirichlet distribution is impractical to use here because the random walk into the physical space—a tiny subspace within the 255-dimensional probability simplex—is extremely inefficient. For the same number of sample points, the Wishart distribution might appear to provide faster convergence than the uniform distribution in terms of N_τ. However, the overall performance using the uniform distribution is practically better. This is because the computation per sample point is about three to four times faster when using the uniform distribution than for the Wishart distribution. A larger sample size helps not only to reduce the statistical error in evaluating sample average quantities like the content; it also makes the random walk, which is set to propagate along the direction given by the covariance matrix of the current sample, more efficient, as the covariance matrix is more accurately estimated when the sample is larger. As a result, the time cost for using the Wishart distribution with $\{N_s = 3 \times 10^4, N_\tau = 3500\}$ is about the same as using the uniform distribution with $\{N_s = 10^5, N_\tau = 3500\}$, but the latter converges better, as is visible in Figure 3b.

The computational time roughly scales as $\mathcal{O}(N_\tau \sqrt{N_s})$ with simple vectorization of the code in Python (version 3.5.7), provided that there is sufficient memory. For the examples shown in Figure 3, the sampling of 10^5 three-qubit states and $N_\tau = 200$ distribution steps took about 2×10^4 s using the Wishart distribution on a regular desktop with no CPU parallelization and 7×10^3 s using the uniform distribution. The sampling of 10^5 four-qubit states and $N_\tau = 3500$ distribution steps using the uniform distribution, which showed good convergence, took about 2.2×10^5 s ($\sim$60 h, which is only about 30 times longer than sampling three-qubit states). We also ran the sampling algorithm for one-qubit and two-qubit states with reliable sample verification. Using the uniform distribution, the sampling of 10^5 one-qubit states and $N_\tau = 10$ takes about 260 s, and the sampling of 10^5 two-qubit states and $N_\tau = 75$ takes about 1.6×10^3 s. Similar scaling of running time was seen in other distributions we sampled. All sampling is conducted on a standard desktop with 8 GB RAM.

In summary, for the SCMC sampling from the state spaces for one to four qubits, which have $(3, 15, 63, 255)$ parameters, the number of required distribution steps is $(10, 75, 200, 3500) \simeq \left(3^{2.1}, 15^{1.6}, 63^{1.3}, 255^{1.5}\right)$, and the computational time is roughly $\left(3^{1.3}, 15^{1.2}, 63^{1.2}, 255^{1.5}\right)$ minutes. The number of distribution steps required for convergence increases as the dimensionality increases, leading to longer computational time, and additional CPU cost is incurred by the multiplication of ever larger matrices. The number of distribution steps, N_τ, is a problem-dependent tuning parameter: Increasing N_τ makes the continuation between intermediate distributions more gradual and gives greater confidence in convergence, but it also increases the running time approximately linearly. In practice, we choose N_τ through short trial runs that balance the observed stabilization of the sample, such as the stabilization of the estimated content, against available computational resources.

For the scaling of the running time, we observe exponents that are approximately independent of the dimension examined, and this suggests that—*within this tested range*—the SCMC algorithm does not exhibit the exponential increase in computation time with respect to dimension that hampers direct rejection sampling. Put differently, the SCMC sampler remains computationally practical as the dimensionality increases, at least for dimensions up to 255. Owing to limited time and computer memory, we did not sample larger quantum systems. However, a powerful work station running the CPU-parallelization version of the code should be able to not only produce a larger sample in a much shorter period of time but also sample quantum states in higher dimensions. These results indicate that further exploration of SCMC in higher-dimensional settings would be worthwhile.

3.3. The Oh–Teo–Jeong Method for Benchmarking

The volume element $(\mathrm{d}\rho)$ in Equation (8) is also the probability element of the uniform distribution, and

$$s_\lambda = \int (\mathrm{d}\rho)\, \eta\big(f(\rho) - \lambda F\big) \tag{9}$$

is the *size* of the λ-region, normalized such that $s_{\lambda=0} = 1$. The relation [52]

$$c_\lambda = \frac{\lambda s_\lambda + \int_\lambda^1 \mathrm{d}\lambda'\, s_{\lambda'}}{\int_0^1 \mathrm{d}\lambda'\, s_{\lambda'}} \tag{10}$$

can be used to obtain an estimate of c_λ from an estimate of s_λ. Owing to the very narrow peak of $f(\rho)$, however, we cannot estimate s_λ by counting how many points of a uniform sample are in the λ-region—there would be far too few sample points in the vicinity of the peak.

The OTJ method introduced in [31,32] offers a clever solution to this problem based on their region-average computation lemma. It provides s_λ by an integration,

$$s_\lambda = s_{\lambda_0} \frac{g_{\lambda_0}}{g_\lambda} \exp\left(- \int_{\lambda_0}^{\lambda} \frac{\mathrm{d}\lambda'}{\lambda' g_{\lambda'}} \right), \tag{11}$$

where g_λ is the average value of $\ln\big(f(\rho)/(\lambda F)\big)$ over the λ-region with respect to the uniform distribution. Although $f(\rho)$ is very narrowly peaked, $\ln\big(f(\rho)\big)$ is not, and g_λ can be estimated accurately by a sufficiently large sample drawn from the uniform distribution over the λ-region, not over the whole quantum state space. Accordingly, an implementation of the OTJ method requires an accurately known reference value s_{λ_0} and a reliable procedure for generating a uniform sample for each λ-region. Both ingredients had problems in the implementation reported in [31,32].

Here, we implement the OTJ method by (i) finding s_{λ_0} from a large uniform sample for λ_0 small enough that, at minimum, a few percent of the sample points are in the λ_0-region and (ii) generating large uniform samples from successive λ-regions using an SCMC algorithm that gradually imposes the constraint $f(\rho) \geq \lambda F$. For the computation of the λ' integral in Equation (11), we discretize linearly in $\ln(\lambda')$.

Figure 4 illustrates aspects of the OTJ algorithm. At the top we see that the λ-regions are not of ellipsoidal shape—the "accelerated hit-and-run" algorithm used in [31,32] assumes that the λ-regions have ellipsoidal shape, which is only justified for $\lambda \lesssim 1$, no such assumptions enter the SCMC algorithm—and that one needs truly tiny positive λ values to enclose a sizable fraction of a uniform sample on the whole state space. The situation is that of a three-outcome measurement in which $A = 2420$ events were observed; see p. 224 in Reference [53]. While this is not a lot of data for a one-qubit measurement, the Bayesian posterior (our target function here) is already peaked extremely narrowly.

At the bottom in Figure 4, we show c_λ for a three-qubit target distribution obtained from sampling directly from the distribution by SCMC (black curve) and by different runs of the OTJ algorithm (colored curves). Figure 4 (bottom) confirms that the SCMC sampling yields the correct c_λ values, as the sequence of OTJ curves converges toward the SCMC curve. This convergence is from below, which tells us that the OTJ estimates of c_λ have a negative bias.

All SCMC runs of the OTJ method proceed from $\lambda = 1$ when all sample points are at the peak location. By reducing λ in N_λ steps, we obtain uniform samples on the respective λ-regions. The "calibration runs" then use $s_{\lambda_0} = 0.024$ for $\lambda_0 = 10^{-250}$, which we get from a large uniform sample on the whole state space, in Equation (11) and the resulting s_λ

in Equation (10). The "precision runs" use $\lambda_1 = 10^{-25}$ instead of λ_0 in Equation (11), with $s_{\lambda_1} \simeq 10^{-24}$ obtained from the calibration runs, and N'_λ intermediate λ values. The graphs for the final calibration run and the first precision run, marked by $*$ in Figure 4 (bottom), are indistinguishable.

Regarding the computational effort, the comparison of the SCMC and the OTJ algorithms speaks strongly in favor of SCMC. The computation time scales roughly as $\mathcal{O}\big((N_\lambda + N'_\lambda)N_\tau\sqrt{N_s}\big)$. Therefore, the final precision run takes about $(2000 + 6000)50 \times\sqrt{10^3}/(200\sqrt{10^6}) \simeq 10^2$ times longer than the direct production of a target sample by SCMC to evaluate c_λ, and the latter has higher accuracy.

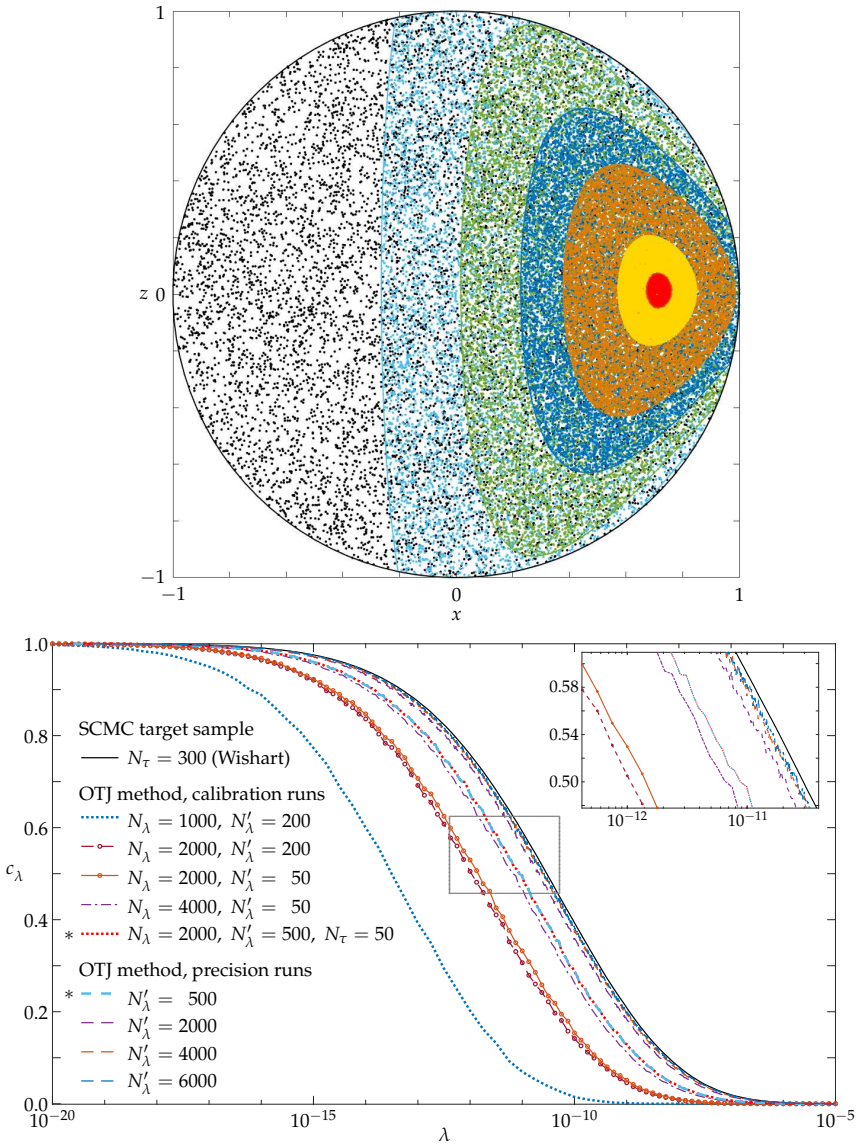

Figure 4. OTJ algorithm illustrated. **Top:** Uniform samples on the λ-regions for single-qubit states on the equatorial disk of the Bloch ball. The target distribution refers to the experimental data of a distorted trine measurement [54] with $(\alpha_1, \alpha_2, \alpha_3) = (1802, 315, 303)$ in Equation (6). The scattered points of different colors mark 10^4 states each in the λ-regions with $\log_{10}(\lambda) = -\infty$, -400, -200, -100, -50, -10, and -1, respectively. The initial distribution ($\lambda = 0$, black points) is uniform on the disk. **Bottom:** Content c_λ evaluated for the three-qubit target distribution of Figure 3a. The black curve is computed directly from a target sample with $N_s = 10^6$ points generated from a Wishart sample by SCMC. The other colored curves show results from several runs of the OTJ algorithm. The inset is a blow-up of the marked rectangular area.

In summary, we can produce samples uniformly distributed in λ-regions by an SCMC implementation of the OTJ method and so evaluate the content c_λ as a function of λ. Our numerical results not only confirm that the OTJ method is viable; they also demonstrate that, for a sharply peaked target distribution, it is more efficient to evaluate the content from the target sample produced directly by SCMC than to use the more involved OTJ method. Further, we observe that the content estimate obtained by the OTJ method has a negative bias.

4. Conclusions

In conclusion, we presented an algorithmic study of the reliability and practical efficiency of the SCMC sampler for sampling quantum states through three explicit examples; yet another application of SCMC is reported in Reference [55]. In the first example, we produce samples of bound entangled states for dimensions 3×3, 3×4, 3×5, and 4×4. For some of these cases, no such samples were available before, and our method can also provide bound entangled states for higher dimensions. For example, we obtain nearly ten thousand two-qutrit bound entangled states in a few minutes through SCMC sampling, whereas several days of independent sampling yield 24 such states from 10^{10} candidates. We also observe that the 2×4 system is particular, as we could not find bound entangled states that obey the PPT-CCNR double criterion. Based on the numerical evidence, we conjecture that such states do not exist.

In the second example, we use the SCMC method for sampling quantum states in accordance with given target distributions for three-qubit and four-qubit systems. For the cases studied, SCMC is substantially more efficient than the alternatives we considered, and its cost appears to grow only moderately over the tested range as the dimension increases.

The third example is an SCMC implementation of the OTJ method for producing uniform samples on regions bounded by values of the target function (the λ-regions); the shortcomings of the original implementation are avoided. We find that, for the purpose of estimating the content of the λ-regions, direct SCMC sampling from the target distribution is much more efficient, and the values obtained by the OTJ method have a negative bias.

The SCMC sampler can be applied to many other sampling problems of quantum systems as long as the constraints can be described by inequalities. For example, one could produce samples of states that violate an inequality of the Bell kind. Multiple constraints can be efficiently applied in parallel. Moreover, due to the well-known channel–state duality, SCMC sampling can also be used to sample channels. We invite the readers to apply the method to their specific sampling problems.

Author Contributions: Conceptualization, all authors; Methodology, all authors; Software, W.L. and R.H.; Formal analysis, all authors; Data curation, W.L. and R.H.; Writing—original draft, all authors; Writing—review & editing, all authors; All authors have read and agreed to the published version of the manuscript.

Funding: J.S. acknowledges support by the National Natural Science Foundation of China (Grant No. 11805010) and the Beijing Institute of Technology Research Fund Program for Young Scholars. The Centre for Quantum Technologies is a Research Centre of Excellence funded by the Ministry of Education and the National Research Foundation of Singapore.

Institutional Review Board Statement: Not applicable.

Informed Consent Statement: Not applicable.

Data Availability Statement: The codes used for the numerical computations are available upon request.

Acknowledgments: We would like to thank David Nott for his insightful advice on SMC. B.-G. E. is extremely grateful for the long-standing support from the Centre for Quantum Technologies, where his share of the work was conducted.

Conflicts of Interest: Authors Rui Han and Berthold-Georg Englert own BiQut as partners. The remaining authors declare that the research was conducted in the absence of any commercial or financial relationships that could be construed as a potential conflict of interest.

Abbreviations

The following abbreviations are used in this article:

CCNR	Computational Cross Norm and Realignment
CPU	Central Processing Unit
ESS	Effective Sample Size
GB	Giga Byte
HMC	Hamiltonian Monte Carlo
PPT	Positive Partial Transpose
MC	Monte Carlo
MCMC	Markov Chain Monte Carlo
OTJ	Oh, Teo, and Jeong
RAM	Random-Access Memory
SCMC	Sequentially Constrained Monte Carlo
SMC	Sequential Monte Carlo

Appendix. SCMC Algorithm

Generally speaking, one would implement SCMC as follows. First, try to generate a sample that is of considerable size. Pick the distribution step according to the scaling with the dimension d of the parameter space, i.e., $\propto d^{1.5}$ (see the last paragraph in Section 3.2). Then, construct the intermediate distributions according to the recipe in Equation (1). Parameterize the inequalities imposed on the target sample in accordance with Equation (2). By trial and error, adjust the Markov chain step size to reach an acceptance rate around 23.4%. Perhaps check the convergence by increasing the number of intermediate distributions; once convergence is ensured, optimize for efficiency by reducing the number of intermediate distributions.

The general algorithm takes in a set of N_s initial sample points with distribution $g(\mathbf{x})$ and finds a discretized sequence of density distributions $\{h_i(\mathbf{x})\}$ that "smoothly" bridges between $g(\mathbf{x})$ and $f(\mathbf{x})$. $\{h_i(\mathbf{x})\}$ takes into account both the change of the probability density distribution and the incorporation of the soft constraints given by Equation (1) to Equation (3).

In general, there can be N_{MC} MCMC iterations between each distribution step, and importance resampling is performed whenever the effective sample size (ESS) drops below a chosen threshold N_{thres}. We employ the iteration kernel in the Metropolis algorithm, which results in sample points with updated weights for the kth iteration $w_i^{(k)} \propto \left[h_i(\mathbf{x}_i^{(k)})\right] / \left[h_{i-1}(\mathbf{x}_i^{(k)})\right]$. The ESS, that is $\mathrm{ESS}^{-1} = \sum_{k=1}^{N_s} \left[w_i^{(k)}\right]^2$, is a measure of sample degeneracy [56], i.e., a small ESS indicates that only a small portion of the sample points are filtered into the next step. This degeneracy can be greatly suppressed in SMC with finer distribution steps as compared with MCMC. In addition, the SMC algorithms can be conveniently implemented with parallel computation for speed-up. The general outline of our SCMC algorithm is given on the next page.

SCMC Sequentially constrained Monte Carlo algorithm

Generate an initial sample $\{\rho^{(1:N_s)}\}$ with distribution $g(\rho)$
Assign weight $w_0^{(k)} = 1/N_s$ for $k = 1 : N_s$
for $i = 1 : N_\tau$ **do**
  Evaluate $h_i(\rho^{(1:N_s)})$ with indicators $I_{\kappa,i}(\rho^{(1:N_s)})$
  for $j = 1 : N_{\mathrm{MC}}$ **do**
    if $j = 1$ **then**
      Update $w_i^{(k)} = w_{i-1}^{(k)} \frac{h_i(\rho^{(k)})}{h_{i-1}(\rho^{(k)})}$ for $k = 1 : N_s$
      Normalize $w_i^{(k)}$
      Calculate ESS $= \left[\sum_{k=1}^{N_s} \left(w_i^{(k)}\right)^2\right]^{-1}$
      if ESS $< N_{\mathrm{thres}}$ **then**
        Importance resampling according to $w_i^{(1:N_s)}$
        Reset $w_i^{(1:N_s)} = 1/N_s$
      end if
    end if
    Propagate $\{\rho^{(1:N_s)}\}$ with MCMC transition kernels
    Accept/reject the new points
  end for
end for

Figure A1 illustrates a simple one-dimensional example of SMC. The target distribution $f(x)$ has two peaks, and we sample it by starting with random samples drawn from a single-peak normal distribution $g(x)$. A simple example that illustrates how the physicality constraint can be effectively imposed is shown in Figure A2. The reference sample is uniform in the probability simplex of the distorted trine measurement of Reference [54] on a single-qubit system and it is filtered through $N_\tau = 10$ intermediate constrained uniform distributions, thereby imposing the physicality constraint by taking $\kappa(\rho)$ to be the smallest eigenvalue of the density matrix of state ρ.

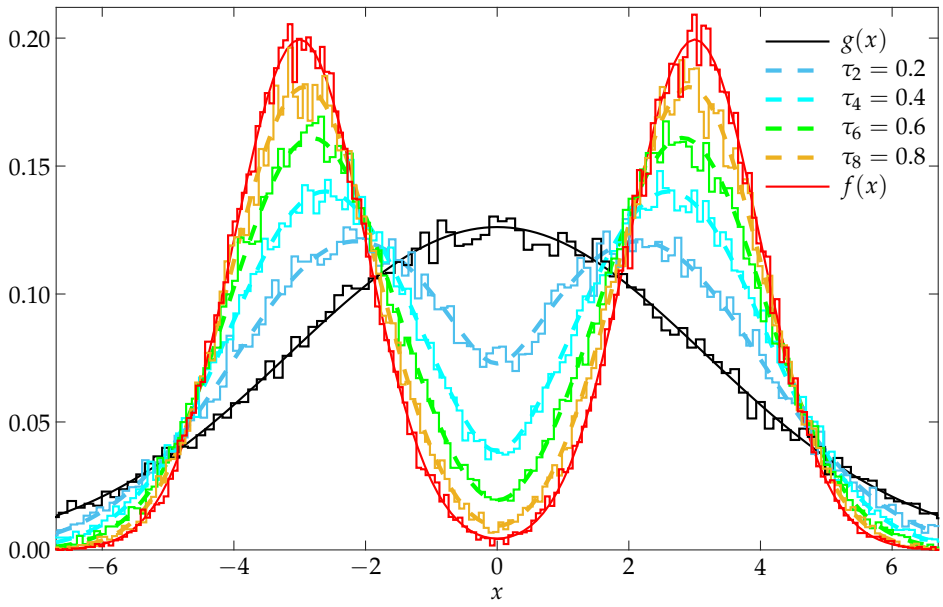

Figure A1. A simple illustration of SCMC in 1D. A single-peak reference sample is used to sample a target distribution with two peaks. The intermediate distributions are given by Equation (1) with $N_\tau = 10$. Both the exact and the numerically estimated distribution for 10^4 sample points are shown.

The computational efficiency of the SCMC algorithms depends on a set of parameters—the number of reference sample points N_s, the number of distribution steps N_τ, the number of Markov chain iterations N_{MC} that the entire sample is advanced by a kernel of choice in each distribution step (see below) and the scaling parameter a—which need to be calibrated for the sampling problem at hand. For most of the examples presented in this paper, we fix $N_{\mathrm{MC}} = 15$ and adjust other parameters in accordance with the criterion set out in Reference [57].

Generally, the number of Markov chain iterations, N_{MC}, is chosen according to [57], $N_R = \lceil \log_{1-ar}(q) \rceil$, where N_R is the required number of Markov chain steps such that there is a $(1-q)$ probability that each point is moved at least once during the Markov chain procedure, which has an acceptance rate of ar. To put in some numbers for illustration, $N_{\mathrm{MC}} = 7$ when $q = 0.01$ and $ar = 0.25$ for a typical Metropolis–Hastings Markov chain, which has a most efficient acceptance rate of 0.234 [58], and we choose $N_{\mathrm{MC}} = 15$ for convenience throughout the paper.

Regarding the choice of kernel, the most standard Gaussian kernel is an option. The kernel we are using here is the "adaptive Metropolis kernel" of Section 2 in Reference [59], which has its origin in Reference [60].

To reduce the sample degeneracy without compromising its efficiency by too much, we set the threshold of ESS at $N_{\mathrm{thres}} = \frac{4}{5} N_s$ and importance resampling is executed once ESS falls below N_{thres}. The sample correlation resulting from importance resampling is attended to by the Markov chain iterations that follow. To reduce the correlation from the final importance resampling before the SCMC algorithm ends, we filter the system through 20 additional Markov chain iterations.

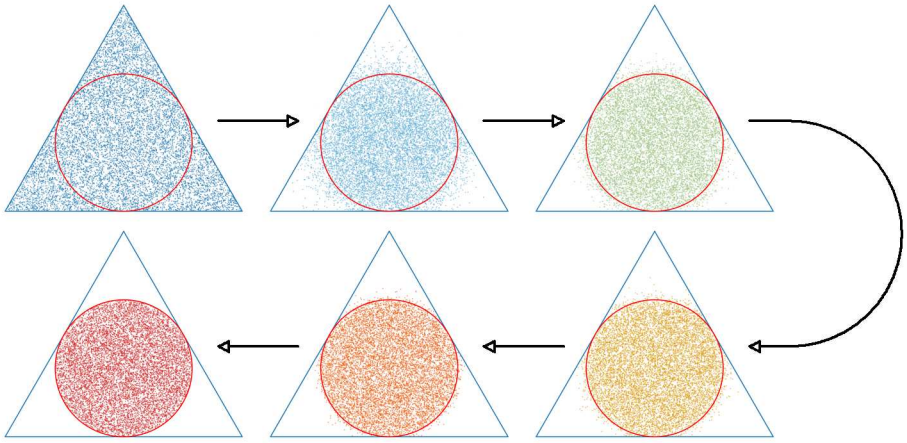

Figure A2. The physicality constraint is gradually imposed through $N_\tau = 10$ intermediate distribution steps. The triangle represents the boundary of the probability simplex, while the circle represents the boundary of the physical region. The distributions are shown for the initial sample (uniform on the simplex, **top left**, $\tau_0 = 0$), for the final sample (uniform on the unit disk, **bottom left**, $\tau_{10} = 1$), and for four intermediate samples ($\tau_i = i/10$ with $i = 2, 4, 6, 8$).

References

1. Hradil, Z. Quantum-state estimation. *Phys. Rev. A* **1997**, *55*, R1561–R1564. [CrossRef]
2. Řeháček, J.; Teo, Y.S.; Hradil, Z. Determining which quantum measurement performs better for state estimation. *Phys. Rev. A* **2015**, *92*, 012108. [CrossRef]
3. Wiebe, N.; Granade, C. Efficient Bayesian phase estimation. *Phys. Rev. Lett.* **2016**, *117*, 010503. [CrossRef]
4. Horodecki, K.; Horodecki, M.; Horodecki, P.; Leung, D.; Oppenheim, J. Unconditional Privacy over Channels which Cannot Convey Quantum Information. *Phys. Rev. Lett.* **2008**, *100*, 110502. [CrossRef] [PubMed]
5. Hamma, A.; Santra, S.; Zanardi, P. Quantum Entanglement in Random Physical States. *Phys. Rev. Lett.* **2012**, *109*, 040502. [CrossRef]
6. Dupuis, F.; Fawzi, O.; Wehner, S. Entanglement Sampling and Applications. *IEEE Trans. Inf. Theory* **2015**, *61*, 1093–1112. [CrossRef]

7. Lund, A.P.; Bremner, M.J.; Ralph, T.C. Quantum sampling problems, Boson Sampling and quantum supremacy. *NPJ Quantum Inf.* **2017**, *3*, 15. [CrossRef]
8. Bouland, A.; Fefferman, B.; Nirkhe, C.; Vazirani, U. On the complexity and verification of quantum random circuit sampling. *Nat. Phys.* **2019**, *15*, 159–163. [CrossRef]
9. Arute, F.; Arya, K.; Babbush, R.; Bacon, D.; Bardin, J.C.; Barends, R.; Biswas, R.; Boixo, S.; Brandao, F.G.S.L.; Buell, D.A.; et al. Quantum supremacy using a programmable superconducting processor. *Nature* **2019**, *574*, 505–510. [CrossRef]
10. Donoho, D.L. *High-Dimensional Data Analysis: The Curses and Blessings of Dimensionality*; AMS Math Challenges Lecture; Research-Gate: Berlin, Germany, 2000; pp. 1–32.
11. Wootters, W.K. Random quantum states. *Found. Phys.* **1990**, *20*, 1365–1378. [CrossRef]
12. Bengtsson, I.; Życzkowski, K. *Geometry of Quantum States: An Introduction to Quantum Entanglement*; Cambridge University Press: Cambridge, UK, 2006. [CrossRef]
13. Osipov, V.A.; Sommers, H.J.; Życzkowski, K. Random Bures mixed states and the distribution of their purity. *J. Phys. A* **2010**, *43*, 055302. [CrossRef]
14. Życzkowski, K.; Penson, K.A.; Nechita, I.; Collins, B. Generating random density matrices. *J. Math. Phys.* **2011**, *52*, 062201. [CrossRef]
15. Collins, B.; Nechita, I. Random matrix techniques in quantum information theory. *J. Math. Phys.* **2016**, *57*, 015215. [CrossRef]
16. Wishart, J. The generalised product moment distribution in samples from a normal multivariate population. *Biometrika* **1928**, *20A*, 32–52. [CrossRef]
17. Goodman, N.R. Statistical analysis based on a certain multivariate complex gaussian distribution (An introduction). *Ann. Math. Stat.* **1963**, *34*, 152–177. [CrossRef]
18. Goodman, N.R. The distribution of the determinant of a complex Wishart distributed matrix. *Ann. Math. Stat.* **1963**, *34*, 178–180. [CrossRef]
19. Han, R.; Li, W.; Bagchi, S.; Ng, H.K.; Englert, B.-G. Uncorrelated problem-specific samples of quantum states from zero-mean Wishart distributions. *arXiv* **2021**, arXiv:2106.08533. [CrossRef]
20. Hastings, W.K. Monte Carlo sampling methods using Markov chains and their applications. *Biometrika* **1970**, *57*, 97–109. [CrossRef]
21. Neal, R.M. MCMC using Hamiltonian dynamics. In *Handbook of Markov Chain Monte Carlo*; Steve, B., Andrew, G., Meng, G.L.J., Eds.; Chapman & Hall/CRC: Boca Raton, FL, USA, 2011; Chapter 5, pp. 113–162.
22. Shang, J.; Seah, Y.L.; Ng, H.K.; Nott, D.J.; Englert, B.-G. Monte Carlo sampling from the quantum state space. I. *New J. Phys.* **2015**, *17*, 043017. [CrossRef]
23. Seah, Y.L.; Shang, J.; Ng, H.K.; Nott, D.J.; Englert, B.-G. Monte Carlo sampling from the quantum state space. II. *New J. Phys.* **2015**, *17*, 043018. [CrossRef]
24. Golchi, S.; Campbell, D.A. Sequentially constrained Monte Carlo. *Comput. Stat. Data Anal.* **2016**, *97*, 98–113. [CrossRef]
25. Del Moral, P.; Doucet, A.; Jasra, A. Sequential Monte Carlo samplers. *J. R. Stat. Soc. B* **2006**, *68*, 411–436. [CrossRef]
26. Doucet, A.; Freitas, N.; Gordon, N. (Eds.) *Sequential Monte Carlo Methods in Practice*; Springer: New York, NY, USA, 2001. [CrossRef]
27. Chopin, N. A sequential particle filter method for static models. *Biometrika* **2002**, *89*, 539–552. [CrossRef]
28. Granade, C.E.; Ferrie, C.; Wiebe, N.; Cory, D.G. Robust online Hamiltonian learning. *New J. Phys.* **2012**, *14*, 103013. [CrossRef]
29. Huszár, F.; Houlsby, N.M.T. Adaptive Bayesian quantum tomography. *Phys. Rev. A* **2012**, *85*, 052120. [CrossRef]
30. Ralph, J.F.; Maskell, S.; Jacobs, K. Multiparameter estimation along quantum trajectories with sequential Monte Carlo methods. *Phys. Rev. A* **2017**, *96*, 052306. [CrossRef]
31. Oh, C.; Teo, Y.S.; Jeong, H. Probing Bayesian credible regions intrinsically: A feasible error certification for physical systems. *Phys. Rev. Lett.* **2019**, *123*, 040602. [CrossRef]
32. Oh, C.; Teo, Y.S.; Jeong, H. Efficient Bayesian credible-region certification for quantum-state tomography. *Phys. Rev. A* **2019**, *100*, 012345. [CrossRef]
33. Available online: https://github.com/feuerbutter/QSCMC (accessed on 25 May 2026).
34. Gekman, A.; Meng, X.L. Simulating normalizing constants: From importance sampling to bridge sampling to path sampling. *Stat. Sci.* **1998**, *13*, 163–185. [CrossRef]
35. Neal, R.M. Annealed importance sampling. *Stat. Comput.* **2001**, *11*, 125–139. [CrossRef]
36. Horodecki, M.; Horodecki, P.; Horodecki, R. Mixed-state entanglement and distillation: Is there a "bound" entanglement in nature? *Phys. Rev. Lett.* **1998**, *80*, 5239–5242. [CrossRef]
37. Hiesmayr, B.C.; Popp, C.; Sutter, T.C. Bipartite bound entanglement. *Int. J. Quantum Inf.* **2025**, *23*, 2530003. [CrossRef]
38. Moroder, T.; Gittsovich, O.; Huber, M.; Gühne, O. Steering bound entangled states: A counterexample to the stronger Peres conjecture. *Phys. Rev. Lett.* **2014**, *113*, 050404. [CrossRef] [PubMed]
39. Tendick, L.; Kampermann, H.; Bruß, D. Activation of nonlocality in bound entanglement. *Phys. Rev. Lett.* **2020**, *124*, 050401. [CrossRef]

40. Horodecki, M.; Horodecki, P.; Horodecki, R. Separability of mixed states: Necessary and sufficient conditions. *Phys. Lett. A* **1996**, *223*, 1–8. [CrossRef]
41. Horodecki, K.; Horodecki, M.; Horodecki, P.; Oppenheim, J. Locking entanglement with a single qubit. *Phys. Rev. Lett.* **2005**, *94*, 200501. [CrossRef]
42. Czekaj, L.; Przysiężna, A.; Horodecki, M.; Horodec ki, P. Quantum metrology: Heisenberg limit with bound entanglement. *Phys. Rev. A* **2015**, *92*, 062303. [CrossRef]
43. Chen, K.; Wu, L.A. A matrix realignment method for recognizing entanglement. *Quantum Inf. Comput.* **2003**, *3*, 193–202. [CrossRef]
44. Horodecki, P. Separability criterion and inseparable mixed states with positive partial transposition. *Phys. Lett. A* **1997**, *232*, 333–339. [CrossRef]
45. Bennett, C.H.; DiVincenzo, D.P.; Mor, T.; Shor, P.W.; Smolin, J.A.; Terhal, B.M. Unextendible product bases and bound entanglement. *Phys. Rev. Lett.* **1999**, *82*, 5385–5388. [CrossRef]
46. Bruß, D.; Peres, A. Construction of quantum states with bound entanglement. *Phys. Rev. A* **2000**, *61*, 030301. [CrossRef]
47. Kay, A. Optimal detection of entanglement in Greenberger–Horne–Zeilinger states. *Phys. Rev. A* **2011**, *83*, 020303. [CrossRef]
48. Kye, S.H. Three-qubit entanglement witnesses with the full spanning properties. *J. Phys. A Math. Theor.* **2015**, *48*, 235303. [CrossRef]
49. Sentís, G.; Eltschka, C.; Siewert, J. Quantitative bound entanglement in two-qutrit states. *Phys. Rev. A* **2016**, *94*, 020302. [CrossRef]
50. Halder, S.; Sengupta, R. Construction of noisy bound entangled states and the range criterion. *Phys. Lett. A* **2019**, *383*, 2004–2010. [CrossRef]
51. Sindici, E.; Piani, M. Simple class of bound entangled states based on the properties of the antisymmetric subspace. *Phys. Rev. A* **2018**, *97*, 032319. [CrossRef]
52. Shang, J.; Ng, H.K.; Sehrawat, A.; Li, X.; Englert, B.-G. Optimal error regions for quantum state estimation. *New J. Phys.* **2013**, *15*, 123026. [CrossRef]
53. Nott, D.J.; Seah, M.; Al-Labadi, L.; Evans, M.; Ng, H.K.; Englert, B.-G. Using prior expansions for prior-data conflict checking. *Bayesian Anal.* **2021**, *16*, 203–231. [CrossRef]
54. Len, Y.L.; Dai, J.; Englert, B.-G.; Krivitsky, L.A. Unambiguous path discrimination in a two-path interferometer. *Phys. Rev. A* **2018**, *98*, 022110. [CrossRef]
55. Bera, A.; Bae, J.; Hiesmayr, B.C.; Chruściński, D. On the structure of mirrored operators obtained from optimal entanglement witnesses. *Sci. Rep.* **2023**, *13*, 2045–2322. [CrossRef]
56. Liu, J.S.; Chen, R. Sequential Monte Carlo methods for dynamic systems. *J. Am. Stat. Assoc.* **1998**, *93*, 1032–1044. [CrossRef]
57. Drovandi, C.C.; Pettitt, A.N. Estimation of parameters for macroparasite population evolution using approximate Bayesian computation. *Biometrics* **2011**, *67*, 225–233. [CrossRef]
58. Roberts, G.O.; Rosenthal, J.S. Optimal scaling for various Metropolis–Hastings algorithms. *Stat. Sci.* **2001**, *16*, 351–367. [CrossRef]
59. Roberts, G.O.; Rosenthal, J.S. Examples of Adaptive MCMC. *J. Comput. Graph. Stat.* **2009**, *18*, 349–367. [CrossRef]
60. Haario, H.; Saksman, E.; Tamminen, J. An adaptive Metropolis algorithm. *Bernoulli* **2001**, *7*, 223–242. [CrossRef]